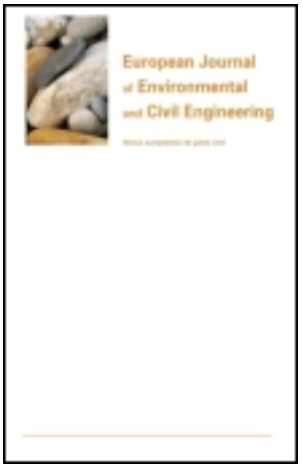

European Journal of Environmental and Civil Engineering
Publication details, including instructions for authors and subscription information:
http://www.tandfonline.com/loi/tece20

Elasto-plastic analysis of the pressuremeter test in granular soil - part 2: numerical study

J. Monnet [a]
[a] Joseph Fourier University, Grenoble, France
Published online: 18 May 2012.

To cite this article: J. Monnet (2012): Elasto-plastic analysis of the pressuremeter test in granular soil - part 2: numerical study, European Journal of Environmental and Civil Engineering, 16:6, 715-729

To link to this article: http://dx.doi.org/10.1080/19648189.2012.667654

European Journal of Environmental and Civil Engineering
Vol. 16, No. 6, June 2012, 715–729

Taylor & Francis
Taylor & Francis

Elasto-plastic analysis of the pressuremeter test in granular soil – part 2: numerical study

J. Monnet*

Joseph Fourier University, Grenoble, France

In the first paper, part 1, we presented the elasto-plastic theory for the expansion of the pressuremeter in granular soil. This theory allows determination of the behaviour of the granular soil around the pressuremeter with only four mechanical parameters. It is compared with previous theory on the dataset of the pressuremeter test on Ticino sand. In the second paper, part 2, we present the numerical analysis of the theoretical conventional limit pressure compared with the result of the Mohr–Coulomb non-standard model used by the Plaxis finite element program. The theoretical evolution of the conventional limit pressure as a function of the variation of each parameter shows a correct agreement with the numerical results. Conclusions are drawn on the influence of these parameters on the pressuremeter results.

Dans un premier article, partie 1, nous présentons la théorie élasto-plastique de l'expansion de la sonde dans le sol granulaire. Cette théorie permet de déterminer le comportement du sol granulaire autour du pressiomètre avec seulement quatre paramètres mécaniques. Nous comparons ensuite ses résultats à ceux de théories plus anciennes pour l'étude des essais pressiométriques réalisés dans le sable de Ticino. Dans un second article, partie II, nous réalisons l'étude analytique de l'évolution de la pression limite donnée par cette théorie et nous la comparons à la valeur numérique trouvée avec le logiciel Plaxis L'évolution de la pression limite en fonction de la variation de chacun de ses paramètres montre un accord raisonnable avec les résultats numériques de Plaxis. Nous concluons sur l'importance relative de ces paramètres sur la pression limite

Keywords: pressuremeter; analysis; granular soil; limite pressure; finite element; validation

Mots-clés: pressiomètre; analyse; sol granulaire; pression limite; éléments finis; validation

1. Introduction

The pressuremeter is a well-known apparatus, widely used for foundation engineering (Amar, Clarke, Gambin, & Orr, 1991; Clarke, 1996; Clough, Briaud, & Hughes, 1990; Gambin, 1990; Ménard, 1957). A general presentation of this technique can be found in Cassan (2005) and Dalton (2005). Its use relies on a set of empirical rules (DTU 13.12, 1988; French Standard NF P 94–110., 2000; French Standard P 94–250-1, 1996) for foundation design. A pressuremeter test may also be considered as an *in situ* shearing test, to measure soil properties using theories of cavity expansion (Fahey, 2005; Monnet & Khlif, 1994; Monnet & Allagnat, 2002; Silvestri, 2001). The main interest of this

*Email: jmonnet@ujf-grenoble.fr

ISSN 1964-8189 print/ISSN 2116-7214 online

http://dx.doi.org/10.1080/19648189.2012.667654
http://www.tandfonline.com

approach is the measurement of soil deformability and shear resistance *in situ*, performed in any type of soil, without sampling. This avoids problems of grain size distribution and disturbance of the soil after sampling, often encountered in samples used for laboratory testing. In this paper, the finite element program Plaxis V.8 is used to calculate the limit pressure under different mechanical conditions and to compare it with the predicted value of the Monnet (2012) theory so that an estimation of the precision of the theory is possible.

2. Method used for the determination of soil parameters from the pressuremeter measurements

The first step is the determination of the interparticle angle of friction on a drained triaxial test carried out on a remoulded sample. The relation in Equation (1) is applied with plastic deformations assumed to be in the dilatancy part of the triaxial test as proposed previously (Frydman, Zeitlen, & Alpan, 1973). The deformation $d\varepsilon_m^p$ corresponds to σ_{oct} (where σ_{oct} is the first invariant of the stress tensor, $1/3\ (\sigma'_1 + \sigma'_2 + \sigma'_3)$) and $d\varepsilon_d^p$ corresponds to τ_{oct} (where τ_{oct} is the second invariant of the stress tensor, $1/3\sqrt{(\sigma'_1 - \sigma'_2)^2 + (\sigma'_2 - \sigma'_3)^2 + (\sigma'_3 - \sigma'_1)^2}$; σ'_1, σ'_2, σ'_3 are effective principal stresses). The measurement of the initial ordinate of the regression line allows the measurement of the interparticle angle of friction. The soil tested (Figure 1) is a marine sand sampled near Bordeaux (France) and the measured value of Φ_μ is 28° with the proposed method.

$$\frac{\tau_{oct}}{\sigma_{oct}} = tg.\Phi_\mu - \frac{d\varepsilon_m^p}{d\varepsilon_d^p}, \tag{1}$$

where ε_m is the first invariant of the strain tensor, $1/3(\varepsilon_1 + \varepsilon_2 + \varepsilon_3)$, and ε_d is the second invariant of the strain tensor, $1/3\sqrt{(\varepsilon_1 - \varepsilon_2)^2 + (\varepsilon_2 - \varepsilon_3)^2 + (\varepsilon_3 - \varepsilon_1)^2}$, and ε_1, ε_2, ε_3 are principal deformations.

The second step is the determination of the angle of friction Φ with the pressuremeter test. The measurement of slope δ (Figure 2) of the linear pressuremeter relationship

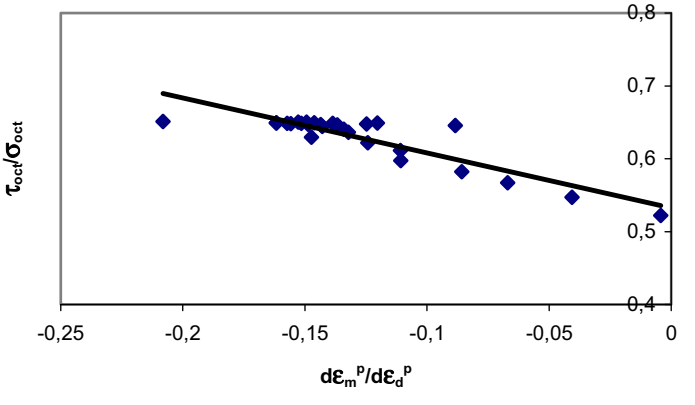

Figure 1. Measurement of the interparticle angle of friction on a remoulded sample on Bordeaux marine sand, drained triaxial test.

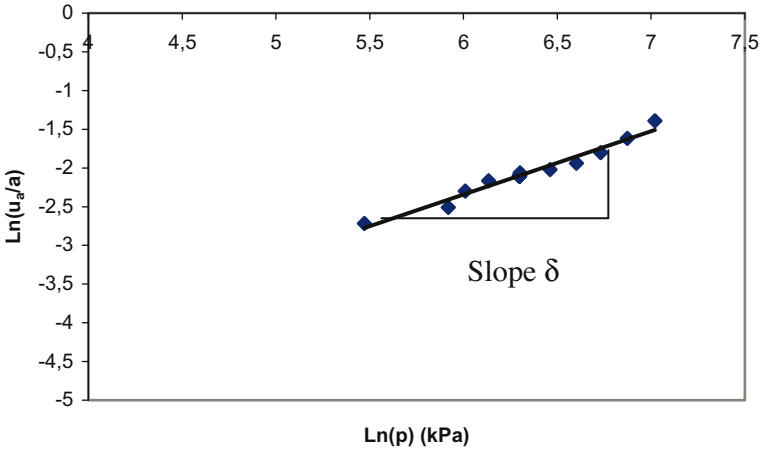

Figure 2. Linear transformation of the pressuremeter relationship for a test in Bordeaux marine sand, borehole PR2, 10 m depth.

between the logarithms of pressure and circumferential borehole deformation at the borehole wall is a function of only two mechanical parameters, the friction angle Φ' and the interparticle angle of friction Φ_μ, as shown in Equations (2) to (5) from Monnet (2012). The knowledge of δ and Φ_μ allows the determination of the angle of internal friction Φ':

$$\delta = \frac{1+n}{1-N}, \tag{2}$$

where:

$$N = (1 - \sin \Phi')/(1 + \sin \Phi'), \tag{3}$$

$$n = (1 - \sin \psi)/(1 + \sin \psi), \tag{4}$$

and

$$\sin \psi = \frac{3.\sqrt{2}\left(\frac{2.\sin \Phi'.\sqrt{2}}{3-\sin \Phi'} - \tan\Phi_\mu\right)}{4 + \sqrt{2}\left(\frac{2.\sin \Phi'.\sqrt{2}}{3-\sin \Phi'} - \tan\Phi_\mu\right)} \tag{5}$$

Φ' is the drained friction angle, and Ψ is the dilatancy angle

The third step is the control of the friction angle Φ' by a comparison between the theoretical curve and the experimental one. The value of Φ' is put into Equation (6) or (7) from Monnet (2012) to draw the theoretical pressuremeter curve, which is compared with the experimental one (Figure 3). Equation (6) is related to an equilibrium with a vertical and horizontal plasticity and Equation (7) is related to only horizontal plasticity. The slope of the unloading reloading is used to measure Young's modulus assuming a classical value of Poisson's ratio of 0.3. The fit between experiment and analysis must be precise on the unloading–reloading sequence so that the Young's modulus should be controlled. This condition introduces an initial translation (Figure 3) of the theoretical

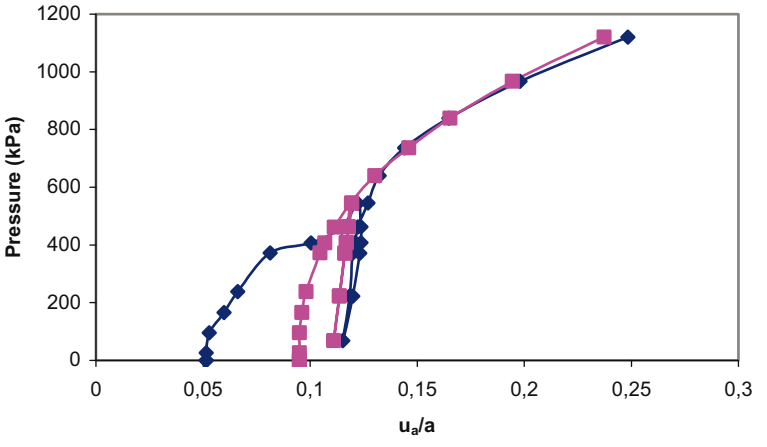

Figure 3. Control of the stress deformation parameters for a pressuremeter test in Bordeaux marine sand, borehole PR2, 10 m depth, E = 80 MPa, ν = 0.42, $\Phi_{\mu} = 28°$, $\Phi' = 32°$.

curve, which can be considered as the plastic effect induced by the pre-drilled technique with the unloading linked to the drilling and the reloading linked to the introduction of the pressuremeter probe which inflates until the horizontal at rest pressure is reached. The correct fitting of the two curves must be precise above the creep pressure to control the angle of friction. The accurate matching of the two curves means that the set of stress–deformation parameters is correct for the theoretical representation of the pressuremeter test.

$$Ln\left[\frac{u_a}{a}(1+n)-C_1\right]=\delta.Ln(p)-\delta.Ln(\gamma.z)+Ln\left[(1-K_0).(\gamma.z.)\frac{(1+n)}{2.G}-C_1\right] \quad (6)$$

with C1=...

$$C_1=\frac{n.(\frac{u_a}{a}).(1+n).(\frac{\gamma.z}{p})^{\delta}+(1+n).(N-K_o).\frac{\gamma.z}{2.G}}{1+n.(\frac{\gamma.z}{p})^{\delta}}$$

$$Ln\left[\frac{u_a}{a}(1+n)-C_1\right]=\delta.Ln(p)-\delta.Ln\left[\frac{2.K_0.\gamma.z}{(1+N)}\right]+Ln\left[K_0.\gamma.z\frac{(1-N).(1+n)}{2.G.(1+N)}-C_1\right], \quad (7)$$

with C1=...

$$C_1=\frac{K_o.\gamma.z.(1-N).(n-1)}{2.G.(1+N)}$$

where a is borehole radius, u_a is displacement at the borehole wall, G is Shear modulus.

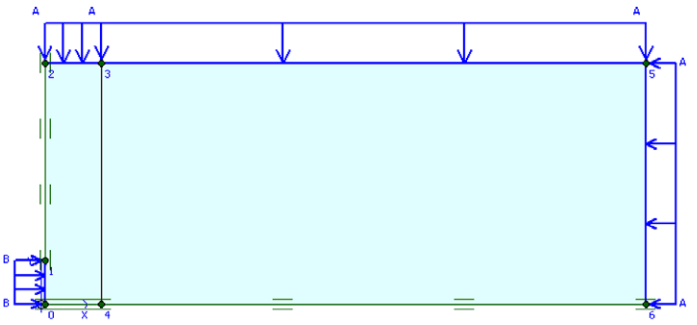

Figure 4. The boundary conditions of the finite element mesh in the vertical plane for a ratio L/D = 20. The borehole is at the left of the figure.

3. Numerical study for the elasto-plastic analysis

3.1. *Boundary conditions and mesh used*

The mesh represents an axisymetric volume of soil around a 3 cm borehole radius (Figure 4). The mesh is drawn with a 5 m external radius and a 2 m vertical thickness. The horizontal lower limit is a mid-plane for the pressuremeter length. There is no vertical displacement allowed on the lower boundary of the mesh. There is no horizontal displacement allowed along the left vertical border at the borehole wall above the pressuremeter to represent tube casing. To simulate a test deeper than 2 m, a vertical stress is applied at the top of the mesh (load A). The horizontal pressure at rest is applied at the vertical right boundary with a K_0 condition (load A). The soil is assumed without weight. The pressuremeter applies a radial stress (load B) at the lower part of the borehole with an imposed stress at each loading step.

The elements (Figure 5) are smaller close to the borehole (cluster 1) than far from it (cluster 2). The L/D ratio is 6 (with L the length and D the diameter of the pressuremeter probe), close to the dimension of the most commonly pressuremeter apparatus used. The displacement along the measurement cell calculated for the conventional limit pressure is chosen for a cross surface of the probe which is twice the original one, and which gives a circumferential deformation of $(\sqrt{2}-1)$, taken to be equal to 0.414.

3.2. *Effect of the probe geometry*

The analysis is carried out with a small strain so that a comparison is possible with the theory that assumes a small strain. The concept of this numerical analysis is:

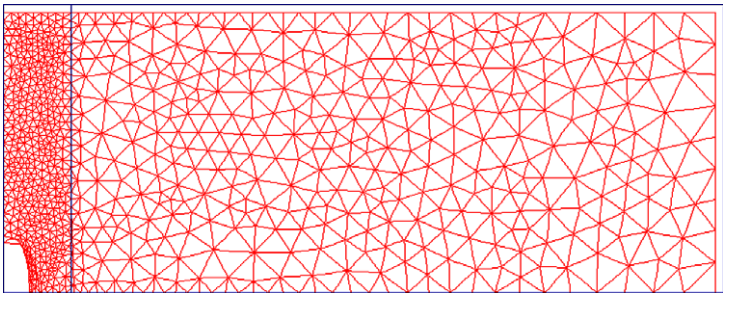

Figure 5. The deformed mesh with displacements scaled 20 times.

- to check if there are only six parameters (E, ν, Φ', Φ_u, σ_z, K_0) which have an influence on the pressuremeter curve (where E is Young's modulus, ν is Poisson's ratio); and
- to check if the influence of these parameters is correctly taken into account by the theory, and if the variation of these parameters gives a predictable variation of the limit pressure.

As the two methods assume a linear-elastic perfectly plastic non-associated Mohr–Coulomb model there should be just a small difference between these two results. The difference comes from the geometry of the probe. When the theory assumes an infinite probe (that is no influence of the L/D dimension of the probe), it integrates the elastic and plastic deformation along the radius. When the Finite Element program takes into account the geometry of the probe, it represents a limited extension of the elastic and plastic area along the radius, but also in the vertical direction. To estimate the influence of the probe geometry, a second finite element calculation was carried out with an L/D ratio equal to 200 (Figure 6), which can be considered to have a behaviour close to an infinite probe and close to the theoretical behaviour. It can be seen (Figure 7) that the theory is very close to the numerical result for the L/D ratio equal to 200, and that the numerical result for the L/D ratio equal to 20 is stiffer. This difference in the limit pressure between the numerical (with L/D = 20) and the theoretical limit pressure is also observed in Figures 10 to 19 (see below). An observed discrepancy of 20% to 25% (Figure 7) should be a maximum so that there should be a limited influence of the geometry of the probe on the limit pressure.

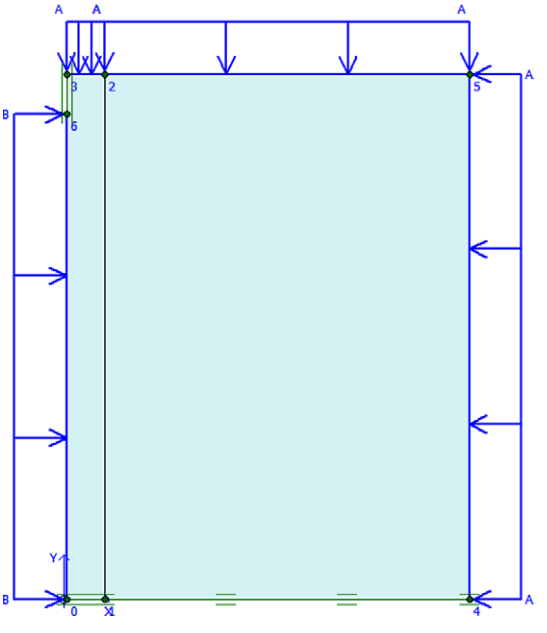

Figure 6. The boundary conditions of the finite element mesh in the vertical plane for a ratio L/D = 200. The borehole is at the left of the figure.

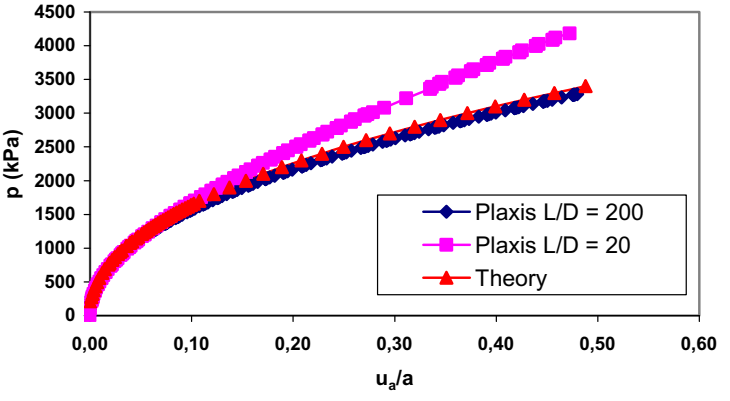

Figure 7. Effect of the probe geometry. Plaxis results for a ratio L/D = 20 and L/D = 200 compared with the theoretical results (E = 65 MPa, ν = 0.3, $\Phi_\mu = 32.2°$, $\Phi' = 40°$, K_0 =: 1.

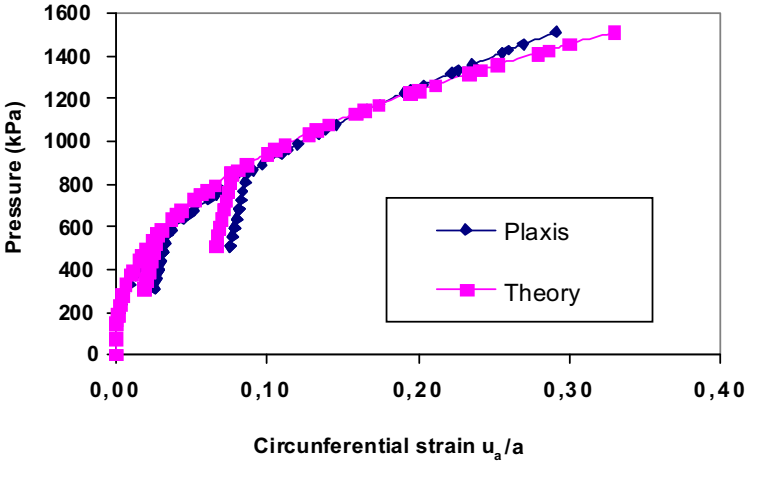

Figure 8. Comparison between finite element and theory, stress–strain relation (E = 40 MPa, ν = 0.3, Φ_μ=29°, $\Phi' = 41°$.

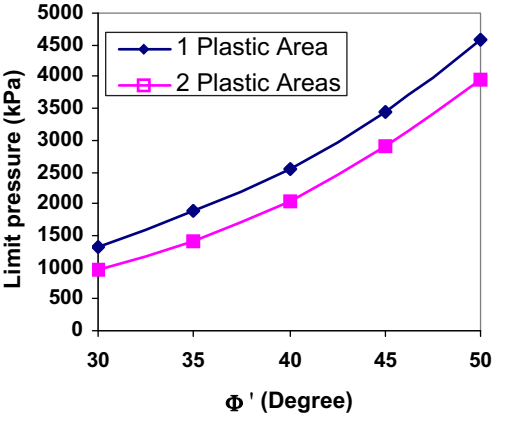

Figure 9. The evolution of the conventional limit pressure as a function of the friction angle.

3.3. Method used to control the theory

The correct adjustment between the theoretical and numerical curves from the beginning to the end involves a lot of points and the objective to carry out a variation of each parameter involves many more points. It is not possible to manage such a large amount of results, so it was decided to simplify this study by using only one point of the pressuremeter curve, which is the conventional limit pressure. This value can be obtained by a direct theoretical and numerical analysis for an expansion of the pressuremeter probe, which is double the initial volume. The theoretical limit pressure equations are Equation (8) for horizontal and vertical plasticity, and Equation (9) for horizontal plasticity only (Monnet, 2012):

$$p'_1 = \gamma'.z.\left(\frac{[(1+n).(\sqrt{2}-1)-C_1]2.G}{[(1-K_0).(1+n).\gamma'.z-2.G.C_1]}\right)^{(1/\delta)} \tag{8}$$

$$p'_1 = \frac{2.K_0.\gamma'.z}{(1+N)}\cdot\left(\frac{[(1+n).(\sqrt{2}-1)-C_1]2.G.(1+N)}{K_0.\gamma'.z.[(1-N).(1+n)-2.G.C_1.(1+N)]}\right)^{(1/\delta)}, \tag{9}$$

where p'_l is the effective conventional limit pressure

The numerical and analytical results are also compared with the relation proposed by the 'Comité Technique Régional Européen 4' (Amar et al., 1991) which comes from Ménard correlative experience. This relation is noted CTRE4 in Figures 10 and later.

$$p'_l = 250\left[2\left(\frac{\phi-24}{4}\right)\right] + K_0.\gamma'.z. \tag{10}$$

3.4. Mechanical parameters and model used

The model used is a standard linear-elastic perfectly plastic non-associated Mohr–Coulomb model of Plaxis. As the theory assumes a small strain, the numerical calculation is carried out with a small strain. The mesh is not updated.

The common set of parameters used is E = 40 MPa, $\nu = 0.30$, σ_z=200 kPa, Φ_{μ}=30, Φ=35°. Then we apply a perturbation on one of these parameters, for example on the

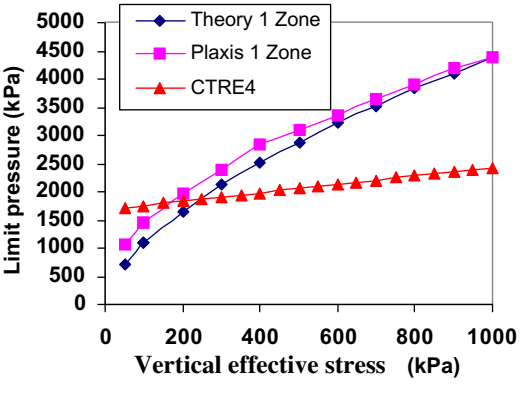

Figure 10. Influence of the vertical stress on the conventional limit pressure with a test involving one plastic zone.

Table 1. Mechanical parameters used in the numerical analysis.

Parameter studied	E (MPa)	γ	G (MPa)	K_0	σ_z (kPa)	Φ_μ	Ψ (°)	Φ' (°)
σ_z – 1 zone	40	0.30	15.38	0.75	50–1000	30	5	35
σ_z – 2 zones	40	0.30	15.38	0.40	50–1000	30	5	35
G – 1 zone	10–100	0.30	3.84–38.4	0.75	200	30	5	35
G – 2 zones	10–100	0.30	3.84–38.4	0.40	200	30	5	35
K_0 – 1 zone	40	0.30	15.38	0.64–1.00	200	30	5	35
K_0 – 2 zones	40	0.30	15.38	0.3–0.63	200	30	5	35
Φ_μ – 1 zone	40	0.30	15.38	0.75	200	10–30	26–5	35
Φ_μ – 2 zones	40	0.30	15.38	0.40	200	10–30	26–5	35
Φ' – 1 zone	40	0.30	15.38	0.75	200	30	0–21	30–50
Φ' – 2 zones	40	0.30	15.38	0.40	200	30	0–21	30–50

Young's modulus so that the shear modulus varies while keeping the others parameters constant (Table 1). Each parameter is studied independently versus the common set of parameters to check its predicted and calculated influence on the limit pressure.

3.5. *Shape of the pressuremeter curve*

In the present study, the pressuremeter test is computed with the common set of parameters (Table 1) of the Plaxis Mohr–Coulomb model (MC). This model uses the linear elastic perfectly plastic model, with a constant dilatancy and a constant angle of friction. The deformation of the borehole is drawn (Figure 8). It appears that the tangent modulus decreases from its maximum initial value until the end of the test. This phenomenon is linked to the progressive increases of the plastic volume zone around the pressuremeter probe, which is shown by the increase of the plastic deformation when unloading–reloading is made at different level of stress (Figure 8). The shape of the theoretical curve is also very close to the finite element results.

3.6. *Influence of the second plastic zone*

The evolution of the conventional limit pressure in Equations (8) and (9) is drawn as a function of the friction angle (Figure 9) for the standard set of parameters. The assumption of plasticity between the vertical stress and the circumferential stress in Equation (9) gives a value of the conventional limit pressure, which is 5% smaller than in the case with only one plastic zone in Equation (8). For the same limit pressure, neglecting the second plastic area in the inverse analysis underestimates the friction angle by a value of 4° (Figure 9). This effect is larger than the sensitivity of the method used for the determination of the mechanical characteristics and must be taken into account.

3.7. *Influence of the vertical stress*

The parameters used in the numerical analysis are shown on lines 2 and 3 in Table 1. The analysis takes into account the vertical stress as the intermediate stress between the radial and the circumferential stress. For granular soil, the conventional limit pressure is then a function of the vertical stress, and when the vertical stress increases, the friction between the radial stress and the circumferential stress leads to an increase of the conventional limit pressure. This variation is described by theoretical Equations (8) and (9)

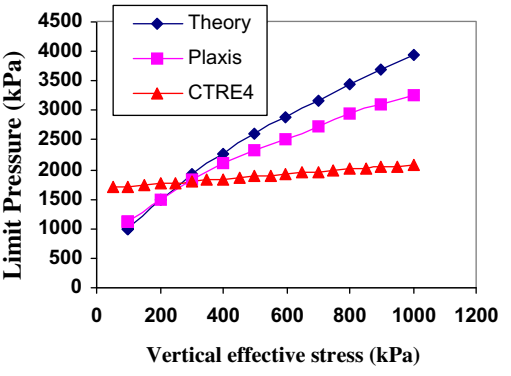

Figure 11. Influence of the vertical stress on the conventional limit pressure with a test involving two plastic zones.

where the vertical stress is a multiplicative factor in the theoretical conventional limit pressure. The finite element method (Figures 10 and 11) shows the same variation of the conventional limit pressure. The distance between the analysis and the Plaxis calculus is in a range of 0 to 20%.

The Ménard correlative (Equation (10)) assumes that the net conventional limit pressure (difference between the conventional limit pressure and the horizontal at rest pressure) does not depend on the vertical stress and appears far from the numerical results (Figures 10 and 11, curve CTRE4). The estimation of the conventional limit pressure by this relation shows a relative distance of –38% to 81% and should be used only in the range of vertical stress between 100 to 300 kPa, where the distance with numerical results remain in a small range lower than 20%.

3.8. *Influence of the shearing modulus*

The parameters used in the numerical analysis are shown on lines 4 and 5 in Table 1 and a variation is applied on the Young's modulus to change the value of the shear

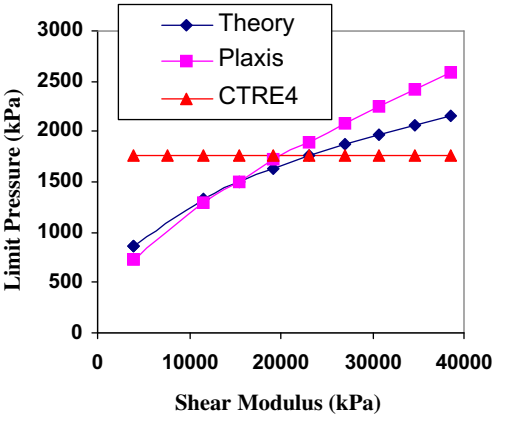

Figure 12. Influence of the shearing modulus on the conventional limit pressure with a test involving one plastic zone.

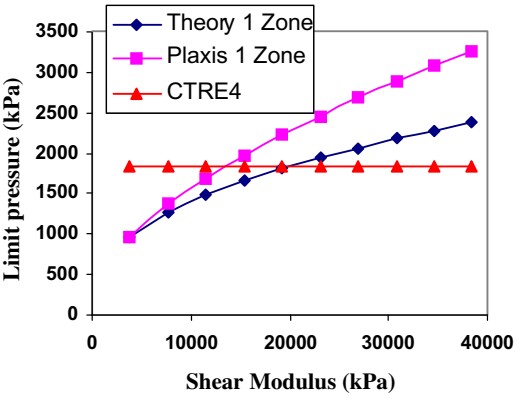

Figure 13. Influence of the shearing modulus on the conventional limit pressure with a test involving two plastic zones.

modulus. The conventional limit pressure is the value of the pressure linked to a volume of the probe, which is twice the initial one. If the soil is stiffer, for a defined value of the pressure, the deformation of the soil should be smaller, and the deformation to twice the initial volume should be reached for a high value of the pressure. On the other hand, for a soft soil, for a defined value of the pressure, the deformation of the soil should be larger, and the deformation to twice the initial volume should be reached for a low value of the pressure. This evolution is predicted by the analysis, and we can see (Figures 12 and 13) that the shearing modulus has an increasing influence on the conventional limit pressure. As the shearing modulus increases, the conventional limit pressure increases. Furthermore, the analysis can predict with a precision of 20% the conventional limit pressure found by the Plaxis program for all cases only for rigid soil (Shear modulus greater than 30 MPa and Young's modulus greater than 70 MPa) and one plastic area.

The correlative relation (Equation (10)) of Ménard assumes that there is no influence of the shearing modulus on the conventional limit pressure and it appears far from the numerical results and completely different.

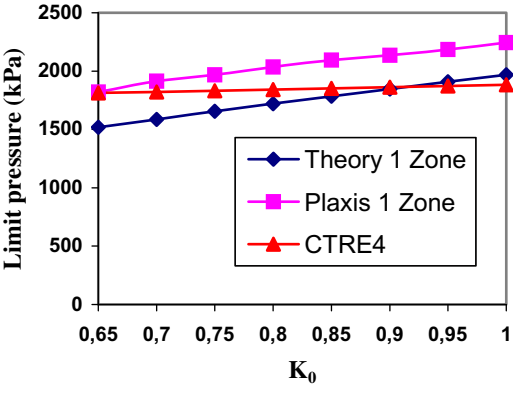

Figure 14. Influence of the K_0 coefficient on the conventional limit pressure with a test involving one plastic zone.

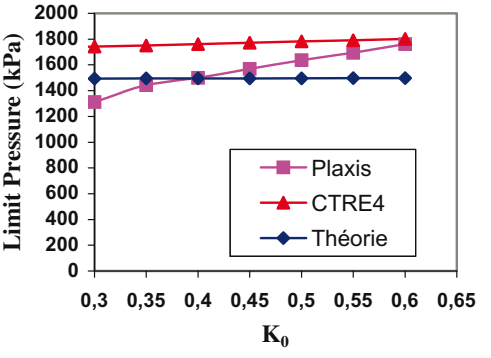

Figure 15. Influence of the K_0 coefficient on the conventional limit pressure with a test involving two plastic zones.

3.9. *Influence of the coefficient of at rest pressure K_0*

The parameters used in the numerical analysis are shown on lines 6 and 7 in Table 1. The coefficient at rest pressure K_0 has a small influence on the conventional limit pressure. An increase of K_0 should increase the horizontal at rest pressure and consequently the conventional limit pressure. This evolution is predicted by the analysis for one plastic area (Figure 14). For two plastic zones (Figure 15) the theoretical conventional limit pressure is found to be constant when the finite element solution shows a small increase. However, the discrepancy between the finite element calculation and the theory remains in a small range (3% to 17%).

The correlative relation (Equation (10)) of Ménard shows also a correct representation of the variation along K_0 value, except for small values (Figure 15) with a discrepancy up to 33%.

3.10. *Influence of the interparticle angle of friction*

The parameters used in the numerical analysis are shown on lines 8 and 9 in Table 1. The interparticle angle of friction varies from 10° for clay to 30° for sand and gravel. The analysis shows that it influences the dilatancy. It can be assumed

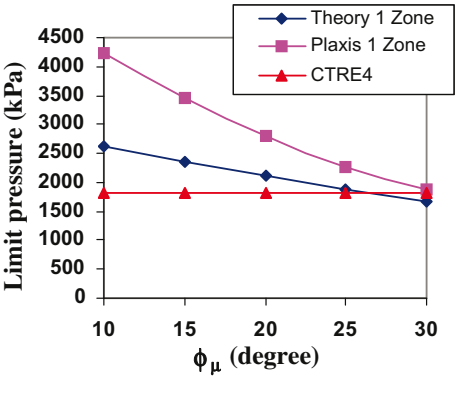

Figure 16. Influence of the interparticle angle on the conventional limit pressure with a test involving one plastic zone.

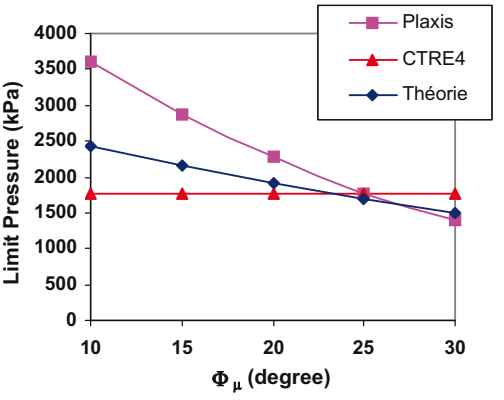

Figure 17. Influence of the interparticle angle on the conventional limit pressure with a test involving two plastic zones.

that an increase of the dilatancy increases the conventional limit pressure because the expansion of the soil increases the volume of the plastic area around the probe. This theoretical phenomenon is described by the analysis (Figure 16 and 17), and when the dilatancy is high (equal to 20° for an interparticle angle of 10° related to a friction angle of 30°), the conventional limit pressure is also high, while when the dilatancy is small (equal to 0° for an interparticle angle of 30° related to a friction angle of 30°) the conventional limit pressure is also small. The discrepancy between the analysis and the finite element results stays in a range of 25% for a value of interparticle angle of friction higher than 20°, which is very common for granular soil. The smallest values could only be found for clays, and in that case the theory cannot be used.

The correlative relation (Equation (10)) of Ménard does not show any evolution of the limit pressure along the interparticle angle and this relation should be used only in a range of values between 25° and 30° where the discrepancy with the numerical results is smaller than 25%.

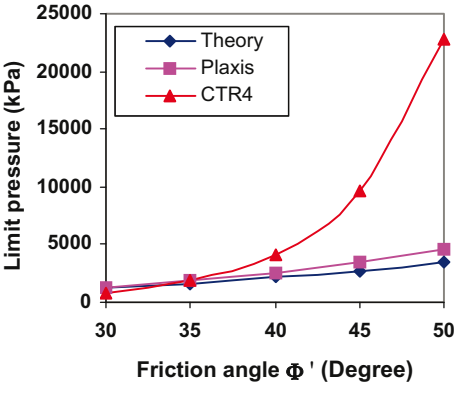

Figure 18. Influence of the friction angle on the conventional limit pressure with a test involving one plastic zone.

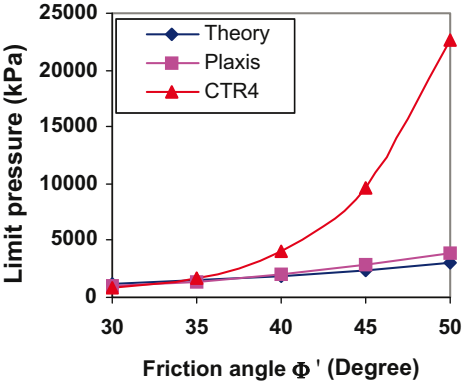

Figure 19. Influence of the friction angle on the conventional limit pressure with a test involving two plastic zones.

3.11. *Influence of the friction angle*

The parameters used in the numerical analysis are shown on lines 10 and 11 in Table 1. The angle of friction acts as a resistance factor of the deformation of the soil, and when the friction angle increases the conventional limit pressure also increases. This is predicted by the analysis where the conventional limit pressure is a function (through the variable N) of the friction angle. This variation is reproduced by the finite element analysis made by Plaxis, and a precise fitting between the analysis and the numerical result is obtained with a maximum error of 24% on the value of the conventional limit pressure (Figures 18 and 19), which validates the analysis for the variation of the friction angle. If we consider the correlative relation of Menard, it can be seen that it gives a large imprecision for an angle of friction larger than 35° with an error which can reach 575%. For a given limit pressure this relation clearly underestimates the friction angle of the soil.

4. Conclusion

We have presented a numerical study of the analysis developed for the interpretation of the pressuremeter test. This new theory takes into account the vertical and the horizontal non-standard elasto-plastic equilibrium around the pressuremeter probe. A plastic behaviour is assumed between the radial stress and the circumferential stress and also between the vertical stress and the circumferential stress.

The analysis shows that four mechanical parameters and the vertical stress have an influence on the pressuremeter results for a granular soil (shearing modulus G, friction angle Φ', interparticle angle of friction Φ_μ, coefficient of at rest pressure K_0). The numerical analysis confirms the influence of these parameters on the conventional limit pressure and shows that they are sufficient to model the pressuremeter test.

The numerical calculation of the pressuremeter test using the Plaxis code has been made with variation of one of these variables, the others remaining unchanged. The numerical results show the same variation as the theory for each parameter and a discrepancy between the values of the limit pressure smaller than 25%. This validates the effect of these parameters on the pressuremeter results.

This analysis shows that plasticity may appear in the vertical plane between the vertical and circumferential stresses. This phenomenon decreases the conventional limit

pressure. The main interest is this study is the fine correlation between the theoretical and numerical value of the limit pressure along the variation of the friction angle. This allows the use of the pressuremeter through the limit pressure as a test to determine the friction angle for common soils.

References

Amar, S., Clarke, B.G.F., Gambin, M., & Orr, T.L.L. (1991). The application of pressuremeter test results to foundation design in Europe. *Comité Technique Régional Européen 4, Pressiomètre*, Rotterdam: A.A. Balkema, pp. 1–24.

Cassan, M. (2005). Les essais pressiométriques et leur applications en France. Rappels historiques et état des connaissances. In M. Gambin, J.P. Magnan, P. Mestat (Eds.). *International Symposium Pressio*, vol. 2, pp. 125–200. Paris: Presses Ponts et Chaussées.

Clarke, B.G. (1996). Pressuremeter testing in ground investigation, Part I: Site operations. *Geotechnical Engineering, 119*, 96–108.

Clough, G.W., Briaud, J.L., & Hughes, J.M.O. (1990). The development of pressuremeter testing. In G.T. Houlsby (Ed.) *3rd International Symposium on Pressuremeters*. London: Thomas Telford, pp. 25–45.

Dalton, C. (2005). United Kingdom experience with pressuremeter 1982–2005. In M. Gambin, J. P. Magnan, P. Mestat (Eds.) *International Symposium Pressio,* Vol. 2. Paris: Presses Ponts et Chaussées, pp. 201–210.

DTU 13-12 (1988). Règles pour le calcul des foundations superficielles, AFNOR DTUP 11-711 Paris: Cahiers du Centre Scientifique et Technique du Bâtiment.

Fahey, M. (2005). Stiffness of sands of differents ages from pressuremeter and seismic cone tests in Perth, in M. Gambin, J.P. Magnan, & P. Mestat (Eds.) *International Symposium Pressio 2005*, Vol. 1 (pp. 611–619). Paris: Presses Ponts et Chaussées.

French Standard NF P 94-110. (2000). *Essai pressiométrique Ménard*. Paris: AFNOR.

French Standard NF P 94-250-1. (1996). *Eurocode 7 Calcul géotechnique*. Paris: AFNOR.

Frydman, S., Zeitlen, J.G., & Alpan, I. (1973). The yielding behaviour of particulate media. *Canadian Geotechnical Journal, 10*, 341–362.

Gambin, M. (1990). The history of pressuremeter practice in France, in G. T. Houlsby (Ed.) *Third International Symposium on Pressuremeters* (pp. 5–24). London: Thomas Telford.

Ménard, L. (1957). An apparatus for measuring the strength of soils in place, Master of Sc. thesis, University of Illinois.

Monnet, J. (2012). An elasto-plastic analysis of the pressuremeter test in granular soil – part 1: theory. *European Journal of Environmental and Civil Engineering*, *16*, 699–714.

Monnet, J., & Allagnat, D. (2002). Design of a large soil retaining structure with pressuremeter analysis. *Geotechnical Engineering, 155*, 71–78.

Monnet, J., & Khlif, J. (1994). Etude théorique et expérimentale de l'équilibre élasto-plastique d'un sol pulvérulent autour du pressiomètre. *Revue Française de Géotechnique, 67*, 3–12.

Plaxis 2D (2010). Brinkgreve, R.B.J., Swolfs, W.M., Engin, E. (Eds.), Delft, Netherlands.

Silvestri, V. (2001). Interpretation of pressuremeter tests in sand. *Canadian Geotechnical Journal, 38*, 1155–1165.